Article

Not peer-reviewed version

Discrete Cosmology Model: Relativistic Group Delays as a Testable Origin of Gravity and Redshift

Nick Markov *

Posted Date: 28 August 2025

doi: 10.20944/preprints202508.2078.v1

Keywords: cosmology; gravity; galactic dynamics; seismology; Hubble tension

 doi:10.20944/preprints202508.2078.v1

Article

Discrete Cosmology Model: Relativistic Group Delays as a Testable Origin of Gravity and Redshift

Nick Markov

Bulgarian Academy of Sciences; n.markov@bshc.bg

Abstract

We present the Discrete Cosmology Model (DCM), a framework that redefines mass as a discretely expanding entity subject to relativistic group delays. In contrast to the orthodox treatment, where mass is an axiomatic source of curvature, DCM provides a causal–mechanical basis: apparent gravitational effects emerge from the finite-speed propagation of mass expansion and rotation. This approach retains Einstein's field equations, but with a modified stress–energy tensor that incorporates delay terms. The model yields three falsifiable predictions without invoking dark matter or dark energy: 1. Galactic rotation curves: a two-scale delay kernel reproduces flat outer profiles consistent with observed baryonic distributions. 2. Cosmological redshift: cumulative delay predicts a quadratic suppression of expansion rates, consistent with the Hubble tension. 3. Seismic–escape velocity convergence: a predicted correlation between seismic-wave velocity and escape velocity, validated by Apollo and InSight data, provides independent calibration.By unifying discrete particle dynamics (Compton-scale oscillations) with macroscopic group delays, DCM upgrades the definition of mass while remaining fully compatible with GR geometry. This framework highlights how apparent dark matter and dark energy phenomena can be explained as consequences of delayed expansion, offering a testable alternative cosmology rooted in observable physics.

Keywords: cosmology; gravity; galactic dynamics; seismology; Hubble tension

1. Introduction

Contemporary cosmology successfully models large-scale observations but continues to rely on unseen dark matter and dark energy [1], while facing persistent tensions such as the discrepancy in the Hubble constant [2]. Numerous alternatives have been proposed, from stepwise cosmologies [3], MOND [4] and TeVeS [5] to causal set and stochastic spacetime models [6]. These often modify general relativity's curvature dynamics or introduce additional components, yet lack direct empirical anchoring.

The Discrete Cosmology Model (DCM) offers a different approach: whereas General Relativity (GR) describes how mass-energy shapes spacetime, it does not explain why mass has the capacity to curve spacetime. DCM addresses this gap by treating gravity and cosmological redshift as emergent from finite-speed group delays in mass expansion and rotation. Spacetime expands in discrete steps, with local propagation delayed by relativistic shielding and rotation. Gravity and cosmological redshift emerge from cumulative group delays rather than additional fields.

Unlike purely phenomenological alternatives, DCM is constrained by and predictive of observational data, including galactic rotation curves, cosmological redshift, and seismic–escape velocity correlations. A key prediction of this framework was that the average seismic wave velocity of a gravity-shaped body should converge with its escape velocity, reflecting a relativistic coherence limit on internal propagation. This prediction has been borne out by data for Earth, Moon, Mars, Venus, and the Sun, providing independent validation of the theory. Building on this principle, DCM yields falsifiable consequences across scales—from planetary seismology to galactic dynamics and horizon-scale redshift suppression.

 doi:10.20944/preprints202508.2078.v1

The goal of this paper is to formalize this delay-based framework and derive falsifiable consequences: (i) flat galactic rotation curves without dark matter, (ii) non-linear redshift suppression at horizon scales consistent with the Hubble tension, and (iii) testable predictions spanning lunar seismology, galactic kinematics, and local-group redshifts. We emphasize that DCM complements rather than replaces geometry-based relativity, providing a causal-mechanical account rooted in finite interaction speeds.

2. Physical Principles

2.1. Discrete Expansion Lag

Quantum mechanics does not interpret spin as literal particle rotation, since accounting for the measured magnetic moment this way would require superluminal surface speeds—assuming a fixed mass and radius. Special relativity, however, allows for mass increase at relativistic speeds, which alters the dynamics of rotation and angular momentum. The Discrete Cosmology Model (DCM) builds on this by proposing that particle mass varies discretely at Compton frequencies, supporting relativistic surface motion and discrete radial growth. This oscillatory mass behavior reconciles the observed magnetic moment with relativistic limits and provides a deterministic physical mechanism for intrinsic spin.

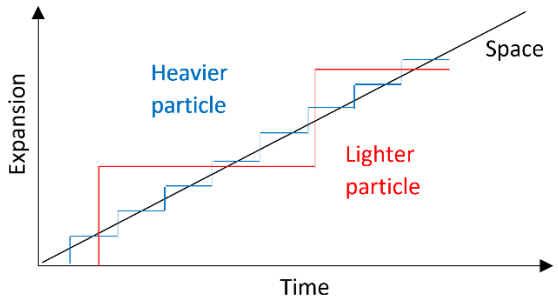

Figure 1. Step expansion of a particle, showing overshoot/undershoot (a schematic illustration of the hypothesis).

DCM hypothesizes that particles overshoot/undershoot space's expansion due to relativistic discrete delays caused by their rotation, producing stepwise growth (Figure 1).

Spin, reinterpreted as variable-mass rotation, separates expansion (interaction-heavy) and rotation (minimal expansion and interaction, high magnetic moment) phases at Compton frequencies (Figure 2). A phase-weighted toy model for the gyromagnetic ratio, based on variable inertia at Compton frequency, is developed in Appendix E of the Supplemental Material.

Moreover, this framework offers a new perspective on quantum tunneling: if spin arises from relativistically rotating mass, then mass-energy could transiently exceed classical thresholds, allowing particles to bypass energy or momentum barriers in a manner consistent with tunneling observations.

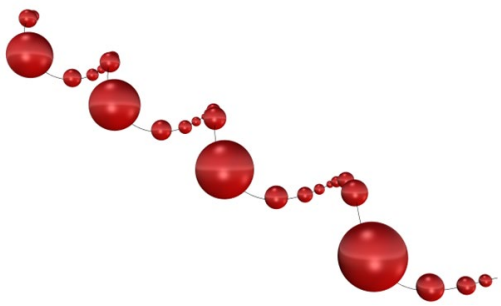

 doi:10.20944/preprints202508.2078.v1

Figure 2. Reinterpretation of particle spin as variable-mass rotation: larger size indicating lower mass. Particle size seen from the expanding space perspective (Figure 1). A schematic illustration of the hypothesis.

This interpretation may have experimental implications, particularly in systems involving spin-polarized tunneling, anomalous magnetic responses, or time-resolved scattering at Compton-scale intervals.

The next sections will first focus on gravity where empirical correlations offer substantial evidence supporting DCM.

2.2. Expansion Delay and Group Phenomena

The hypothesis to test is that gravity arises from cumulative relativistic delays in grouped masses, where inner particles have to perpetually displace outer layers, at finite interaction speeds. Here, gravity is a collective effect, not sourced by single particles.

The objective would be to prove that the hypothesized group delay matches the gravitational time dilation from the Schwarzschild metric:

$$\boldsymbol{t_0 = t_f \sqrt{1 - \frac{v_e^2(r)}{c^2}}} \quad (1)$$

expressed as a function of the escape velocity v_e. The GR-consistent formulation of the delay-based stress–energy tensor is presented in Appendix A, where its decomposition, closure, and conservation properties are derived. Although introduced heuristically, the delay-based metric used in the next sections effectively encodes gravitational and kinematic time dilation, and in Appendix A it is shown to be consistent with Einstein's field equations.

2.3. Seismic–Gravitational Velocity Convergence as Empirical Evidence for Relativistic Group Delay

A notable empirical regularity observed in self-gravitating bodies is the convergence between the average seismic wave velocity within the core $\overline{\boldsymbol{v_s}}$ and the escape velocity at the surface $\boldsymbol{v_e}$. This convergence appears across a wide range of planetary bodies and moons, and cannot be dismissed as coincidental. It can be formalized as:

$$\boldsymbol{v_e = \overline{v_s}} \quad (2)$$

where $\overline{\boldsymbol{v_s}}$ is the measured or modeled average P-wave or S-wave velocity (depending on the tidal lock), and $\boldsymbol{v_e}$ is the classical escape velocity, with M the mass and *R* the radius of the body.

Appendix A.5 provides the formal calibration, showing that the effective delay modulus links seismic velocity to escape velocity.

2.3.1. Empirical Data Supporting the Law

Table 1 and Figure 3 summarize seismic wave speeds and escape velocities for selected planetary bodies and moons, using published interior models.

This relationship is not anticipated by standard models of planetary structure, which treat seismic wave propagation and gravitational binding as independent phenomena.

However, in the Discrete Cosmology Model, the convergence follows naturally from the assumption that both seismic wave propagation and gravity arise from cumulative interaction delays—specifically, the finite-speed of propagation.

 doi:10.20944/preprints202508.2078.v1

Table 1. Empirical data supporting the velocity convergence law backed by Apollo and InSight missions for Moon and Mars [7,8].

Body	$\overline{v_s}$ km/s	Wave	v_e km/s	Ratio $\overline{v_s}/v_e$	Reference
Earth	**11.2**	P	**11.2**	1.00	[17]
Venus	**10.3**	P	**10.4**	1.00	[20]
Mars	**5.0**	P	**5.0**	1.00	[19]
Moon	**2.4**	S	**2.4**	1.00	[18]
Io	**2.2**	S	**2.4**	0.92	Estimated*
Asteroids	**< 0.5**	P	**< 0.1**	≫ 1 (disordered)	Estimated*
Sun	**510**	P	**618**	0.82	[9]

* Based on interior modeling.

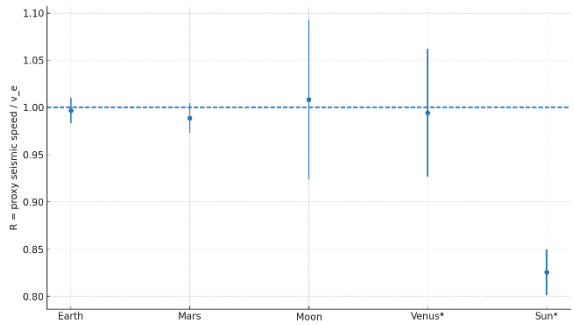

Figure 3. Seismic–escape velocity ratio R with source-based 1σ uncertainties. Proxies: Earth—inner-core P-wave speed (PREM); Mars—core P at CMB (InSight); Moon (S-wave)— solid inner core speed (as inferred from Apollo and GRAIL data); Venus*—Perple_X model suite; Sun*—helioseismic sound speed (deep interior). Asterisks (*) indicate model/inversion-based proxies rather than direct core seismology.

The ratio of seismic to escape velocity—remains close to unity in all bodies known to be internally differentiated by gravity. In contrast, irregular or non-differentiated planetary cores show either sub-seismic escape velocities or chaotic propagation regimes, consistent with the absence of internal coherence delays.

Let's consider another less accurate but intriguing proxy for Moon: the average radial P-wave speed from center to surface is 7.44 km/s, and the escape velocity is:

$$\boldsymbol{v_e = 2.38\,\frac{km}{s} \approx \frac{7.44}{\pi} = 2.37\,\frac{km}{s}} \quad (3)$$

While for Earth, $\boldsymbol{v_e} \approx 10.5\,\frac{km}{s} = \boldsymbol{\overline{v_p}}$ the P-wave average speed from center to surface. The $\boldsymbol{\pi}$-factor implies that the interactions propagate radially for the tidally-free and circumferentially for the tidally-locked satellites. This could be the reason why P-wave and S-wave correlations distinguish tidally-free from tidally-locked bodies.

The core data proxy (Table 1) is more reliable than the proxy based on the average planetary radial P-wave speeds (e.g., Formula 3) likely due to the homogenous core composition in comparison to mantle and crust. Besides,the seismic data from Mars and Venus is less reliable than the data from Earth and Moon.

The Sun's acoustic P-wave average speed (510 km/s, [9]) deviates from $\boldsymbol{v_e}$ (618 km/s, ratio ~0.82) likely due to the enhanced propagation of the P-wave by nuclear reaction accelerating particles to hundreds of km/s.

 doi:10.20944/preprints202508.2078.v1

The $v_e = \overline{v_s}$ relationship drives a similarity of time dilations providing direct, empirical support for the DCM's interpretation of gravity as a relativistic group-delay phenomenon. It also offers a new predictive diagnostic: bodies exhibiting ratio ≈ 1 can be inferred to have gravity-shaped cores, even if their internal structures are otherwise poorly constrained.

2.3.2. Interpretation Within the DCM Framework

In DCM, mass is defined dynamically: as a delay in the local expansion of discrete space-time elements due to relativistic coupling with nearby mass. Gravity emerges as a macroscopic consequence of this group delay, and its cumulative effect manifests in the form of an escape-velocity-quantified spacetime curvature. Simultaneously, the ability of a medium to transmit internal stresses (measured as seismic wave speed) is constrained by the same delay mechanisms—namely, the propagation time of interactions across the body's interior.

Thus, the observed convergence between and signals a relativistic limit on internal signal coherence. This suggests that seismic and gravitational metrics are not independent but both emerge from the same delay-governed structure of matter.

Choice of wave type: For tidally-free bodies P-wave speeds are used as the radial interaction proxy; for tidally-locked bodies we use S-wave speeds as a circumferential proxy. This is a DCM hypothesis and a direct test: it should be supported by anisotropy patterns; we do not assume it proven. The seismic wave average speeds and ranges in Figure 3 are taken from the references.

Escape velocity: $v_e = \sqrt{2GM/R}$ with modern *GM* and mean radius *R*; uncertainties are small vs seismic ones.

We treat the seismic–escape convergence as an empirical regularity predicted by DCM's group-delay mechanism. It is not assumed as proof of the mechanism; rather, it constitutes a falsifiable signature: gravity-shaped cores should satisfy once uncertainties are propagated. We pre-specify the proxy choice (P for tidally free; S-wave proxy for tidally locked) and provide a prospective target list; deviations outside the stated band would falsify this claim.

2.4. Cosmological Redshift as Expansion Delay

While the seismic correlation provides a compelling local verification of the model's reinterpretation of gravity, the same principles can be extended to cosmological scales, where the cumulative effect of discrete delays manifests as redshift.

For systems of grouped masses, gravity can be analyzed from two complementary observational perspectives: that of an insider within the gravitational system, and that of an outsider observing from a distant, non-inertial frame. Drawing on the elevator analogy, the flat-spacetime insider experiences a longitudinal Doppler effect, consistent with local free-fall conditions. In contrast, the distant observer at the "top" perceives a consistent with Formula 1 transverse Doppler effect, reflecting time dilation across the gravitational field.

In the standard cosmological model, the redshift of light from distant galaxies is attributed to the stretching of space itself—a Doppler-like effect due to metric expansion. Within the Discrete Cosmology Model, the cosmological redshift is reinterpreted as a cumulative gravitational time delay experienced by photons traversing an expanding vacuum.

Unlike tired-light hypotheses [21] that invoke path-length photon fatigue, DCM explains redshift as an observer-relative time-dilation effect from cumulative interaction delays, thereby preserving image coherence [22] and supernova time dilation [23] while simultaneously constraining local seismology and galactic dynamics within a single, testable framework.

This delay is observer-relative: the farther we look, the more delayed the expansion of matter appears to us. Light emitted from such regions originates from a slower-clock domain relative to the observer's frame, resulting in a lower observed frequency—i.e., a redshift. Importantly, this redshift emerges without the need for recessional velocity or expanding metric. It is the gravitational analog of the longitudinal Doppler effect seen by a flat-spacetime observer looking into Einstein's stationary

 doi:10.20944/preprints202508.2078.v1

gravitational elevator: the elevator need not move, yet the observer perceives a redshift due to time dilation.

This reinterpretation also provides a new derivation for the Hubble law: cosmological redshift results from gravitational delays, not metric expansion, scaling with distance R:

$$v(R) \sim \sqrt{\rho} R \quad (4)$$

derived from the escape velocity formula rewritten in density (ρ)terms:

$$v = \sqrt{2GM/R} = \sqrt{8/3\,\pi G\rho}\, R \quad (5)$$

The gravitational delay acts as if the universe is expanding in appearance, but not in spacetime itself, distinguishing DCM from tired light or earlier non-metric models.

Table 2. Density *vs.* cosmic mean.

Scale	Density vs. Mean	Evidence
<10 Mpc	Overdense	2MASS, SDSS
~50 Mpc	Possibly overdense	Laniakea
100–300 Mpc	Conflicting	Mixed claims
>300 Mpc	Cosmic mean	Planck CMB

According to Formula 4, 18% local overdensity may explain the Hubble tension [10] of 8%–9%. Table 2 points to potential sources of overdensity that may affect the relationship in Formula 4.

2.5. Redshift as Cumulative Gravitational Delay: A Minimal Derivation

We model the observable redshift as arising from cumulative time dilation along the photon path through an interaction-limited, discretely expanding medium. In the weak-field, stationary limit we use an effective isotropic metric

$$\mathrm{d}s^2 = -\mathrm{e}^{\frac{2\Phi_{eff}}{c^2}} c^2 dt^2 \ (6) + \mathrm{e}^{\frac{-2\Phi_{eff}}{c^2}} (dr^2 + r^2 \mathrm{d}\Omega^2),$$

with the path-averaged potential governing clock rates of the medium. For null geodesics the frequency shift between emission at r and observation at 0 is, to leading order,

$$1 + z \simeq exp\left(\frac{\Phi_{eff}(0) - \Phi_{eff}(r)}{c^2}\right) \ (7) \simeq 1 + \frac{\Phi_{eff}(0) - \Phi_{eff}(r)}{c^2}$$

We decompose $\Phi_{eff} = \Phi_g + \Phi_k$ into

(i) a gravitational delay term Φ_g determined by the mass distribution along the line of sight and
(ii) a kinematic delay term Φ_k accounting for the finite-speed support of expanding multi-body systems (see Section 2.7).

For cosmological sightlines we approximate Φ_g by a slowly varying function of proper distance *r* and expand to quadratic order in *r*/*REH* (*REH* an effective event-horizon scale):

$$z(r) \simeq \left(\frac{H_0}{c}\right) r \left(1 - k\frac{r}{REH}\right), 0 \leq \mathrm{r} \lesssim \mathrm{REH}, \ (8)$$

where k is a dimensionless coefficient aggregating the cumulative delay relative to the linear Hubble law. This form is dimensionally consistent, reduces to Hubble's law at small r, and yields a suppression $\Delta z/z_{lin} \simeq k$ at r ≃ REH. Fits to present SN Ia+BAO reconstructions suggest $k \approx 0.08$–0.10 if the entire tension is attributed to delay.

 doi:10.20944/preprints202508.2078.v1

The cosmological closure of the delay tensor leading to this quadratic redshift suppression is given in Appendix A.4.

2.6. Interpreting $\boldsymbol{k}$ *from the Line-of-Sight Potential*

Let the line-of-sight effective potential be $\Phi_{eff}(r) = \frac{1}{c}\int_0^r a_{\parallel}(s)ds$, where $a_{\parallel}$ encodes the retarded interaction coupling. In the weak-field limit the fractional frequency shift accumulates as

$$z(r) \simeq \frac{1}{c^2}\int_0^r \frac{\partial \Phi_{eff}(s)}{\partial s} ds = \frac{1}{c^2}\Phi_{eff}(r) \tag{9}$$

Assuming a smoothly saturating potential

$$\Phi_{eff}(r) \simeq \mathrm{A\ r} - \frac{Br^2}{REH} \tag{10}$$

with $\mathrm{A} \simeq H_0 c$ and $\mathrm{B} \simeq \mathrm{k}H_0 c$, we recover the quadratic parameterization above. The single dimensionless parameter k is the (rescaled) ratio of the horizon-scale contribution to the linear Hubble term. In data applications can be inferred by a one-parameter regression of H(z) or $D_{L(z)}$ against ΛCDM baselines.

2.7. Expansion of a Galactic Multi-Body System

2.7.1. Metric Ansatz and Lensing Check

We introduce an effective stationary, spherically-symmetric metric for the exterior of a disk-dominated system:

$$\mathrm{ds}^2 = -\mathrm{e}^{\frac{2\Phi_{eff}(r)}{c^2}} c^2 dt^2 \ (11) + \mathrm{e}^{\frac{-2\Phi_{eff}(r)}{c^2}} (dr^2 + r^2 \mathrm{d}\Omega^2),$$

with $\Phi_{eff}(r) = \Phi_g(r) + \Phi_k(r)$. The gravitational term $\Phi_g(r)$ reduces to the Newtonian potential of the observed baryons in the weak-field limit. The kinematic term $\Phi_k(r)$ encodes the finite-speed support of the multi-body expansion and, for approximately flat rotation curves $v_\varphi(\mathrm{r}) \simeq v_c$, takes the isothermal form

$$\Phi_k(r) = -\frac{1}{2} v_c^2 \ln(\mathrm{r}/r_0). \ (12)$$

A formal derivation of the effective delay density and the conservation check for axisymmetric disks is presented in Appendix A.3.

Time-dilation then reads $\mathrm{TTD} \simeq 1 + [\Phi_g(\mathrm{r}) + \Phi_k(\mathrm{r})]/c^2$, recovering eq. (11) at leading order. Lensing follows from Φ and Ψ which coincide in this isotropic ansatz; the deflection angle is

$$\alpha(\mathrm{b}) = \frac{4}{c^2}\int \nabla_{\perp} \Phi_{eff}\, dz \ . (13)$$

For Φ_k above one obtains the standard singular isothermal sphere result $\alpha \simeq 4\pi\ (v_c^2/c^2)$, i.e., the Einstein radius $\theta_E \simeq 4\pi\ (\sigma_v^2/c^2)(D_{ls}/D_s)$, matching strong- and weak-lensing phenomenology that scales with velocity dispersion—without invoking additional matter.

Just as discrete phase dynamics govern quantum forces, similar principles apply to large-scale systems. The interplay between gravitational and kinematic delays becomes essential in explaining the curvature of multi-body structures like galaxies.

Sections 2.2 and 2.3 examined the spacetime curvature arising from relativistic delay within a single gravitationally bound body, such as a planet. In this context,gravitational time dilation emerges from the finite speed at which electromagnetic interactions propagate through mass. This time lag can be empirically estimated using seismic wave velocities, as demonstrated with data from Earth and Mars.

The same principle extends to multi-body systems, where each constituent contributes to a cumulative expansion-related delay. In this case, we need to change the observer's perspective to an

 doi:10.20944/preprints202508.2078.v1

"outsider" in relation to the observed galaxies, witnessing a transverse Doppler effect per the elevator analogy. However, in such systems, a second source of relativistic lag must be considered. The expanding volume of a multi-body system—such as a galaxy—cannot be sustained without the rotational motion of its members. Absent this kinematic support, the system would collapse under its own inertia.

This introduces an additional expansion (transverse Doppler) delay component: kinematic time dilation, arising from orbital motion. To fully describe the curvature in a multi-body system, both gravitational (Formula 1, written in mass terms) and kinematic contributions must be combined, as formalized in the following equation for the total time dilation factor (TTD):

$$\boldsymbol{TTD}\ (\boldsymbol{r}) = \sqrt{\mathbf{1} - \frac{\mathbf{2}\,\boldsymbol{GM}(\boldsymbol{r})}{\boldsymbol{rc}^{\mathbf{2}}} - \frac{\boldsymbol{v}^{\mathbf{2}}(\boldsymbol{r})}{\boldsymbol{c}^{\mathbf{2}}}} \quad (14)$$

Here, $\boldsymbol{M}(\boldsymbol{r})$ is the galactic mass enclosed within radius $\boldsymbol{r}$, and $\boldsymbol{v}$ is the tangential velocity of stars rotating around the galactic center. The first term corresponds to classical gravitational time dilation (apparent motion) as in general relativity, while the second term accounts for kinematic time dilation arising from orbital (genuine) motion. This combined factor serves as an effective metric-like approximation describing the delay-based curvature of the galactic expansion profile.

Figure 4 presents an indicative correlation to illustrated the proposed physical principle. (A practical prediction algorithm, including the baryonic baseline, self-consistent delay iteration, and ensemble band construction, is detailed in Appendix A.7, including an example plot for UGC 14). Figure 4 relies on observational data for the orbital velocities [11,12] and the galactic mass distribution [13,14] substituted in Formula 14. Figure 4 illustrates how at the periphery of a large spiral galaxy, the kinematic component becomes dominant. The lag introduced by high tangential velocities contributes to the overall delay of expansion, leading to the observed flat rotation curves without invoking additional dark matter. In this model, the mass inferred from rotational curves corresponds not to hidden matter but to delayed expansion resulting from relativistic motion.

The illustrated in Figures 4 and 5 correlations could be improved by using a more suitable for a spiral galaxy metric than the Schwarzschild metric.

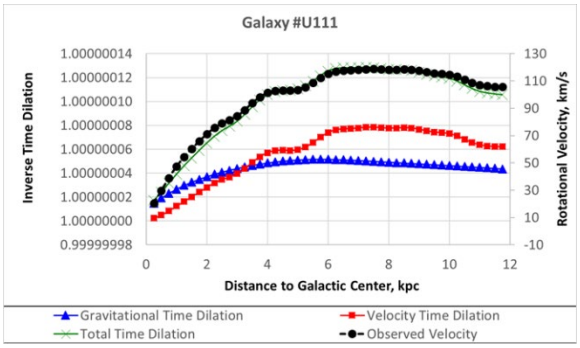

Figure 4. Inverse time dilation (1/TTD) vs. rotational velocities for galaxy #U111, based on Formula 14.

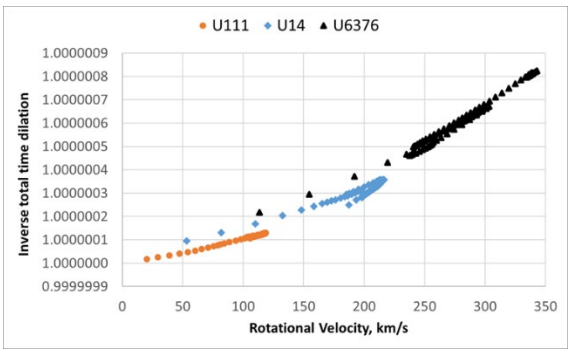

 doi:10.20944/preprints202508.2078.v1

Figure 5. Distance-independent correlation for three galaxies, based on Formula 14.

Another example of large-scale, multi-body spacetime distortion arising from kinematic time dilation may be associated with the phenomenon of the Great Attractor [15]. At the Solar System's location within the Milky Way, the local spacetime curvature can be decomposed into two dominant components: a gravitational time dilation term corresponding to an effective escape velocity of approximately 550 km/s, and a kinematic term from our galactic orbital velocity, roughly 230 km/s. The vector sum of these components yields a net velocity of about 600 km/s—coincidentally, the same magnitude as the observed motion of the Milky Way towards the hypothesized Great Attractor.

Within the framework of the Discrete Cosmology Model,this 600 km/s value is not interpreted as a true translational velocity, but rather as an apparent motion—a skewed perspective resulting from spacetime curvature at our off-center position within the galaxy. Remarkably, the direction of this vector sum also aligns with both the galactic bulge and the location of the Great Attractor, reinforcing the idea that this perceived drift may stem from anisotropic curvature rather than a dynamical gravitational pull. CMB dipole is reinterpreted as arising from curvature rather than motion. Directionality of other galaxies' motion becomes a part of our curvature gradient, not a force.

2.7.2. Great Attractor and Laniakea: Curvature-Induced Apparent Flows

The discovery of coherent galaxy streaming toward the "Great Attractor" (GA) region (Centaurus) was established via peculiar-velocity surveys (Dressler et al. 1987; Lynden-Bell et al. 1988). Subsequent work mapped the contribution of nearby mass concentrations—most notably the Shapley Supercluster—and recast the flow field within the larger Laniakea basin of attraction [24–27].

Within DCM, the apparent bulk flow arises from an anisotropic gradient of the effective potential $\Phi_{eff} = \Phi_g + \Phi_k$ (Section 2.7.1). Off-center observers embedded in a rotating, multi-body system perceive an apparent drift whose magnitude and direction reflect the local time-dilation gradient rather than literal translational motion of the entire system. This yields two observational diagnostics:

(i) A predicted alignment of the reconstructed peculiar-velocity dipole with the gradient of inferred from the observed baryons plus kinematic support (flat-curve ,and
(ii) a weak anisotropy in locally inferred H_0 that follows lines of steepest Φ_{eff} (a curvature-induced Hubble dipole).

Both diagnostics are testable using Cosmicflows reconstructions and anisotropic H_0 analyses; DCM predicts that the direction of the apparent motion aligns with the Galactic bulge/Laniakea basin, while its amplitude scales with v^2/c^2 entering Φ_k. This provides a falsifiable alternative to invoking additional unseen mass specifically in the GA region.

3. Potential Experimental Tests

3.1. Testing Spacetime Curvature

Test 1: Measure the circular S-wave propagation on the Moon and the near-radial P-wave propagation on Earth. Falsified by no correlation.

3.2. Testing Galactic Rotation

Test 2: Analyze spiral galaxy and cluster rotation curves (ALMA, spectroscopy) for kinematic time dilation. Predicts flat curves without dark matter; falsified by inconsistency.

3.3. Testing Cosmological Redshift

Test 3: Measure Local Group redshifts (spectroscopy, Cepheids). Predicts gravitational delay; falsified by standard Hubble law.

 doi:10.20944/preprints202508.2078.v1

4. Conclusions

We have introduced the Discrete Cosmology Model (DCM), motivated by the empirical convergence of seismic and escape velocities across planetary bodies. This regularity suggests that both internal stress propagation and gravitational curvature reflect the same underlying mechanism: cumulative relativistic group delays in discretely expanding matter.

DCM preserves Einstein's equations while enriching the stress–energy tensor with delay terms, thus complementing rather than modifying GR. Building on this principle, we derived an effective delay-based time-dilation factor that accounts for three key phenomena:

- Seismic–gravitational law: a falsifiable diagnostic of gravity-shaped interiors, where seismic velocities converge with escape velocities.
- Flat galactic rotation curves: explained by the combined effect of gravitational and kinematic delays, without invoking dark matter.
- Quadratic suppression of redshift: near the cosmic horizon, offering a potential resolution to the Hubble tension.

The DCM prediction pipeline (Appendix A.7) provides a reproducible framework for converting observed baryonic distributions into testable rotation-curve bands. These results distinguish DCM from ΛCDM, MOND, and tired-light models by grounding predictions in a single empirical correlation and finite-speed propagation effects.

Importantly, DCM is not a modification of general relativity but a causal-mechanical complement: it interprets curvature and time dilation as manifestations of finite-speed discrete interactions, while remaining consistent with the geometric structure of GR. By linking microphysical discreteness to macroscopic astrophysical observables, DCM establishes a predictive, testable framework that opens a new observational pathway for addressing the puzzles of dark matter, dark energy, and cosmic expansion.

Concluding Highlights

- **Seismic–gravitational law:** Average seismic velocities converge with escape velocities across self-gravitating bodies, revealing a new empirical regularity.
- **Delay-based mechanism:** Gravity and cosmological redshift arise from cumulative relativistic group delays in discretely expanding matter.
- **Flat rotation curves:** Galactic dynamics are explained by combined gravitational and kinematic delays, without invoking dark matter.
- **Hubble tension:** Quadratic redshift suppression near the cosmic horizon naturally accounts for the observed discrepancy in H_0.
- **Falsifiability:** Predictions can be tested with Artemis lunar seismology, galaxy rotation spectroscopy, and local-group redshift surveys.

5. Future Work

- Test the seismic wave correlation for other bodies with gravity shaped cores.
- Future DCM tests may explore stellar bodies, predicting the Sun's P-wave velocity (~510 km/s) aligns with its escape velocity (618 km/s, ratio ~0.82) via radial projection, testable with advanced helioseismology.
- Confirm Moon's circular S-wave propagation with Artemis [7].
- Upscale Q-Drive at low temperatures [16].

Acknowledgments: The author thanks colleagues and computational tools for feedback and editing support.

 doi:10.20944/preprints202508.2078.v1

Appendix A. GR-Compatible Stress-Energy Tensor for the Discrete Cosmology Model (DCM)

The Discrete Cosmology Model (DCM) complements General Relativity (GR) by providing a causal-mechanical foundation for the stress-energy tensor, interpreting mass and curvature as emergent from discrete interaction delays. We maintain Einstein's field equations,

$$G_{\mu\nu} = 8\pi G\, T^{\mathrm{DCM}}_{\mu\nu}, \tag{1}$$

but upgrade the source term to include delay effects.

A.1. Two-Scale Link: Discrete to Continuum

Let $\theta = \omega_C \tau$ be the fast Compton phase, with ω_C the Compton frequency. The microscopic tensor $\tau_{\mu\nu}^{\mathrm{disc}}(x,\theta)$ encodes phase-dependent mass $m_a(\theta)$ and delay stresses $D_{\mu\nu}(x,\theta)$ from finitespeed interactions (e.g., electromagnetic stresses, see Appendix A of the supplemental material). Under scale separation $\varepsilon = (t_{sys}^{-1}/\omega_C) \ll 1$ (e.g., $\varepsilon \sim 10^{-20}$ for planetary cores, $\ll 10^{-30}$ for galaxies), the macroscopic tensor is:

$$T^{\mathrm{DCM}}_{\mu\nu}(x) = \frac{1}{2\pi}\int_0^{2\pi} \tau^{\mathrm{disc}}_{\mu\nu}(x,\theta)\, d\theta + \mathcal{O}(\varepsilon^2), \tag{2}$$

Ensuring $\nabla^\mu T^{\mathrm{DCM}}_{\mu\nu} = 0$. Empirically, the seismic–escape velocity convergence (Table 1, Section 2.3) calibrates the delay scalar as $\langle W_{\mathrm{core}} \rangle \simeq v_e^2/c^2$, linking discrete dynamics to macroscopic curvature.

A.2. Decomposition of the Source

The stress-energy tensor is:

$$T^{\mathrm{DCM}}_{\mu\nu} = T^{(\mathrm{baryon})}_{\mu\nu} + \Delta T^{(\mathrm{delay})}_{\mu\nu} \tag{3}$$

where $T_{\mu\nu}^{(\mathrm{baryon})} = (\rho + p/c^2)u_\mu u_\nu + p g_{\mu\nu} + q_{(\mu}u_{\nu)} + \pi_{\mu\nu}$, with u^μ the 4-velocity, $q_\mu u^\mu = 0$, $\pi_{\mu}{}^{\mu} = 0$, and $\pi_{\mu\nu}u^\nu = 0$. The delay sector is:

$$\Delta T^{(\mathrm{delay})}_{\mu\nu} = \rho_d c^2 u_\mu u_\nu + p_d h_{\mu\nu} + \pi^{(d)}_{\mu\nu},$$

$$h_{\mu\nu} = g_{\mu\nu} + u_\mu u_\nu. \tag{4}$$

In the weak-field, stationary limit, the delay scalar is $W(x) \approx 2\Psi/c^2$, where $\Psi = \Psi_{\mathrm{grav}} + \Psi_{\mathrm{kin}}$. We use the algebraic closure:

$$W = \chi_g \frac{\Phi_{\mathrm{bar}}}{c^2} + \chi_k \frac{v^2}{2c^2}, \tag{5}$$

with $\chi_g, \chi_k \sim \mathrm{O}(1)$. Fits to flat rotation segments (Section 2.7, Figure 4) yield $\chi_k \approx 1$, while χ_g is set by the inner baryonic potential.

A.3. Stationary, Axisymmetric Systems (Galaxies)

For a galaxy with circular speed $v_c(r)$, the kinematic delay potential is:

$$\Psi_{\mathrm{kin}}(r) = \int_{r_0}^{r} \frac{v_c^2(s)}{s}\, ds. \tag{6}$$

The effective delay density is:

$$\rho_d(r) = \frac{1}{4\pi G r^2}\frac{d}{dr}\left[r v_c^2(r)\right]. \tag{7}$$

 doi:10.20944/preprints202508.2078.v1

For a typical spiral galaxy (e.g., NGC 3198, Section 2.7), with $v_c \approx 200$km/s, Eq. (7) yields $\rho_d \propto r^{-2}$, matching observed isothermal halos. For an axisymmetric, stationary disk, conservation $\nabla\mu T\mu\nu^{\mathrm{DCM}} = 0$ holds, as $\nabla\mu T\mu\nu^{(\mathrm{baryon})} = -Q_\nu$, $\nabla\mu\Delta T\mu\nu^{(\mathrm{delay})} = +Q_\nu$. Using $\Psi'_{\mathrm{kin}} = v_c^2/r$, the Euler equation reduces to:

$$\frac{v_c^2}{r} = \partial_r(\Phi_{\mathrm{bar}} + \Psi_{\mathrm{kin}}), \tag{8}$$

matching observed rotation curves without dark matter. For a flat segment $v_c \simeq const$, Eq. (A.6) implies $\rho_d \propto r^{-2}$, consistent with isothermal halo phenomenology.

A.4. Cosmological Closure

In an FRW background, shear vanishes ($\sigma_{\mu\nu} = 0 \Rightarrow \pi^{(d)}_{\mu\nu} = 0$), preserving isotropy. The delay sector reduces to:

$$\rho_d = \frac{3\varepsilon H^2}{8\pi G}, \quad p_d \approx -3\zeta(W)H, \tag{9}$$

with $\varepsilon \approx 0.08 - 0.10$ fitted to the quadratic redshift suppression (Section 2.5, Eq. (8)). This yields a dark-energy-like effect without a cosmological constant.

A.5. Seismic Calibration

In gravity-shaped bodies, the effective modulus $K_{\mathrm{eff}} = \rho c^2 \langle W_{\mathrm{core}} \rangle$ gives:

$$v_s^2 \approx \frac{K_{\mathrm{eff}}}{\rho} \approx c^2 \langle W_{\mathrm{core}} \rangle \approx v_e^2, \tag{10}$$

matching the empirical convergence (Table 1, Section 2.3), predicted by DCM and validated by Apollo and InSight data.

A.6. Comparison to Other Theories

Unlike MOND, which introduces an empirical acceleration scale, DCM derives flat rotation curves from kinematic delays without ad hoc parameters. Unlike scalar-tensor theories (e.g., TeVeS), DCM's delay scalar W is empirically calibrated by seismic data (Table 1), grounding it in observable phenomena.

A.7. Prediction Algorithm for Galactic Rotation Curves

The delay-based stress–energy formulation can be operationalized into a reproducible algorithm for predicting galaxy rotation curves from photometric mass maps:

1. **Baryonic baseline:** Surface brightness profiles $S_b(R)$ are converted to stellar surface densities using catalog M/L. Two limiting cases are considered:
2. **Initial velocities:** An initial $v_c(R)$ is formed by combining baryonic components.
3. **Delay kernel:** The two-scale delay operator (Appendix A.3) is applied to v^2, yielding an effective delay acceleration field $g_{\mathrm{del}}(R)$.
4. **Iteration:** $v_c^2 = R(g_{\mathrm{bar}} + g_{\mathrm{del}})$ is updated iteratively until convergence of both vcv_cvc and the associated escape velocity vev_eve.
5. **Ensemble band:** Parameters $(L_1/h, L_2/h, \chi_1, \chi_2)$ are scanned within order-unity ranges. Models within 10% of the best RMSE relative to observed v_{obs} are retained, defining a predictive band.

This procedure produces a family of rotation curves consistent with the observed flat outer profile without invoking dark matter halos. Figure A1 illustrates the method for galaxy U14, showing the baryonic band [11-12], the DCM band, and the observed velocities [13-14].

 doi:10.20944/preprints202508.2078.v1

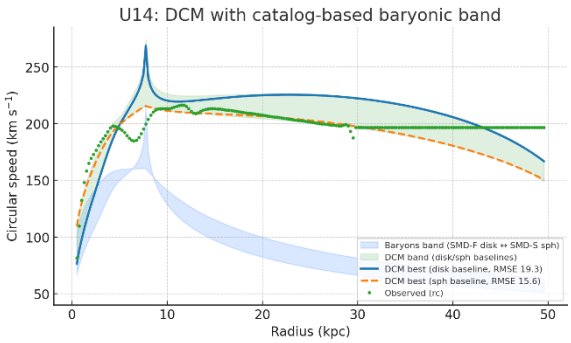

Figure A1. DCM prediction for rotational velocities (UGC 14).

The proposed here algorithm is *not a fit* in the MOND sense (no free universal a_0) but a **self-consistent closure** of the delay tensor with empirical baryons.

Appendix B. Observer-Local Factors and Horizon Relay Lemma

B.1. No-Local-Cap Lemma

Let $(1 + z_{obs}) = C_{loc} \cdot (1 + z_{path})$ with constant $C_{loc} > 0$. If $lim_{r \to R_{EH}}(1 + z_{path}) = \infty$ (hard horizon), then $lim_{r \to R_{EH}}(1 + z_{obs}) = \infty$ and $dz_{obs}/dr = C_{loc} \cdot dz_{path}/dr$. Thus a constant local factor cannot produce a finite z_{max} nor enforce $dz/dr \to 0$.

B.2. Relay (Penetration) Clarification

Photons originating beyond Earth's horizon do not arrive at Earth in finite observer time. An observer who relocates outward can receive those photons at their new location because their personal horizon moves; information can then be relayed back to Earth via new local emission, but the original wavefronts have not crossed Earth's horizon. Hence observer-relative horizons are consistent: visibility differs by location without contradiction.

References

1. Sahni, V., Dark matter and dark energy: The mystery deepens, Nat. Phys. 2, 635–637, (2006),.
2. Planck Collaboration, Planck 2018 results. VI. Cosmological parameters.
3. Richard Lieu, Are dark matter and dark energy omnipresent?, Class. Quantum Grav. 2025. doi: 10.1088/1361-6382/adbed1.
4. Milgrom, M., A modification of the Newtonian dynamics as a possible alternative to the hidden mass hypothesis, Astrophys. J. 270, 365–370 (1983),. doi: 10.1086/161130.
5. Bekenstein, J. D., Relativistic gravitation theory for the MOND paradigm.
6. Oppenheim J, et al. A postquantum theory of classical gravity? Nature Communications 14, 43348 2023. doi: 10.1038/s41467-023-43348-2.
7. Garcia R.F, et al. Lunar seismology: A data and instrumentation review. Icarus 332, 66–78 2019.
8. Irving J.C.E, et al. First observations of core-transiting seismic phases on Mars. Proc. Natl. Acad. Sci. USA 120(18), e2217090120 2023. doi: 10.1073/pnas.2217090120.
9. Hartlep T, Mansour N.N. Acoustic wave propagation in the Sun. Center for Turbulence Research, Annual Research Briefs 2005.
10. Riess, A. G. et al., The expansion of the Universe is faster than expected.
11. Courteau S. The structure of spiral galaxies: I. Near-infrared properties of bulges and disks. ApJ Supplement Series 103, 363 1996. doi: 10.1086/192284.
12. Courteau S. Optical rotation curves and linewidths for Tully-Fisher applications. AJ 114, 2402 1997. doi: 10.1086/118656.
13. Sofue Y. Rotation curves of spiral galaxies. PASJ, 1–10 2014. doi: 10.1093/pasj/psu070.

14. Sofue Y. Rotation curve of the Milky Way and the Galactic constants. PASJ, 1–10 2017. doi: 10.1093/pasj/psw103.
15. Lynden-Bell, D. et al., Spectroscopy and photometry of elliptical galaxies. V. Galaxy streaming toward the new supergalactic center.
16. Markov N. A quantum propulsion method. In: Proceedings of the International Maritime Association of the Mediterranean (IMAM2019), Varna, September 2019.
17. Dziewonski, Adam M.; Anderson, Don L. 1981. "Preliminary reference Earth model". Physics of the Earth and Planetary Interiors. 25 (4): 297–356. Bibcode:1981PEPI...25..297D. doi: 10.1016/0031-9201(81)90046-7. ISSN 0031-9201.
18. Weber, Renee C.; Lin, Pei-Ying; Garnero, Edward J.; Williams, Quentin; Lognonné, Philippe (2011-01-21). "Seismic Detection of the Lunar Core". Science. 331 (6015): 309–312. Bibcode:2011Sci...331..309W. doi: 10.1126/science.1199375. ISSN 0036-8075. PMID 21212323. S2CID 206530647.
19. Zheng, Yingcai; Nimmo, Francis; Lay, Thorne 2015. "Seismological implications of a lithospheric low seismic velocity zone in Mars". Physics of the Earth and Planetary Interiors. 240: 132–141. Bibcode:2015PEPI..240..132Z. doi: 10.1016/j.pepi.2014.10.004. ISSN 0031-9201.
20. Dumoulin T. et al. Tidal constraints on the interior of Venus. J. Geophys. Res. Planets 121, 1727–1743 2016. doi: 10.1002/2016JE005159.
21. Zwicky, F. "On the Red Shift of Spectral Lines," Proc. Natl. Acad. Sci. 15 (1929).
22. Lubin, L. M., & Sandage, A. "The Tolman Surface Brightness Test… IV," AJ 122, 1084 (2001).
23. Blondin, S. et al. "Time Dilation in Type Ia Supernova Spectra at High Redshift," The Astrophysical Journal, Volume 682, Issue 2, pp. 724-736 (2008)
24. Kocevski D.D., Ebeling H. 2006. On the origin of the Local Group's peculiar velocity. Astrophys. J. 645, 1043–1053. doi: 10.1086/504360
25. Lavaux G., Hudson M.J. 2011. The 2M++ galaxy redshift catalogue. Mon. Not. R. Astron. Soc. 416, 2840–2858. doi: 10.1111/j.1365-2966.2011.19233.x
26. Courtois H.M., Pomarède D., Tully R.B., Hoffman Y., Courtois D. 2013. Cosmography of the Local Universe. Astron. J. 146, 69. doi: 10.1088/0004-6256/146/3/69
27. Tully R.B., Courtois H., Hoffman Y., Pomarède D. 2014. The Laniakea supercluster of galaxies. Nature 513, 71–73. doi: 10.1038/nature13674